

Ab Initio Study of the Mechanical, Thermal and Optoelectronic Properties of the Cubic CsBaF₃

M. HARMEL^a, H. KHACHAI^a, A. HADDOU^a, R. KHENATA^b, G. MURTAZA^{c,*}, B. ABBAR^d,
S. BIN OMRAN^e AND M. KHALFA^a

^aLaboratoire d'Etude des Matériaux et Instrumentations Optiques, Université Djillali Liabes Sidi Bel-Abbès, Algérie

^bLaboratoire de Physique Quantique et de Modélisation Mathématique de la Matière (LPQ3M),
Université de Mascara, 29000 Mascara, Algérie

^cMaterials Modeling Lab, Department of Physics, Islamia College University, Peshawar, Pakistan

^dLaboratoire de Modélisation et Simulation en Sciences des Matériaux, Physics Department,
Djillali Liabès University of Sidi Bel-Abbès, Sidi Bel-Abbès 22000, Algérie

^eDepartment of Physics and Astronomy, Faculty of Science, King Saud University,
P.O. Box 2455, Riyadh 11451, Saudi Arabia

(Received May 24, 2013; in final form June 16, 2014)

We have investigated the structural, elastic, electronic, optical and thermal properties of CsBaF₃ perovskite using the full-potential linearized augmented plane wave method within the generalized gradient approximation and the local density approximation. Moreover, the modified Becke–Johnson potential (TB-mBJ) was also applied to improve the electronic band structure calculations. The ground state properties such as lattice parameter, bulk modulus and its pressure derivative were calculated and the results are compared with the available theoretical data. The elastic properties such as elastic constants, anisotropy factor, shear modulus, Young's modulus and Poisson's ratio are obtained for the first time. Electronic and bonding properties are discussed from the calculations of band structure, density of states and electron charge density. The contribution of the different bands was analyzed from the total and partial density of states curves. The different interband transitions have been determined from the imaginary part of the dielectric function. The thermal effect on the volume, bulk modulus, heat capacities C_V and the Debye temperature was predicted using the quasi-harmonic Debye model, in which the lattice vibrations are taken into account.

DOI: [10.12693/APhysPolA.128.34](https://doi.org/10.12693/APhysPolA.128.34)

PACS: 62.20.de, 65.40.Ba, 65.40.De

1. Introduction

Understanding of physical properties of materials for their useful applications has always been a prime field of interest. Materials scientists even in today's technologically advanced society are still struggling for chief and efficient materials. Perovskites family contains a large number of compounds ranges from insulators to superconductors and from diamagnetic to colossal magnetoresistive (CMR) compounds. They are also preferable for the lens materials because it does not have birefringence that makes design of lenses difficult. Furthermore, perovskite structure has an area for studding some physical properties like giant magnetoresistance [1], nearly zero temperature coefficient of resistivity [2] and laser source [3]. The fluoroperovskites structure ABF₃ is one of the common structures of the perovskite. The A and B elements are alkali metals and alkaline earth metals, respectively. Fluoroperovskite compounds have many applications due to their unique properties of tunable laser [4], crystal fields [5] electron–phonon interactions [6, 7] as well as phase transition behaviours [8] and

other physical properties, such as ferroelectricity [9], antiferromagnetism [10], and semiconductivity [11]. Moreover, the fluoroperovskite compounds can be used in the medical field to measure the dose during radiation therapy, and they may also be used in the manufacture of radiation imaging plates for X-rays, gamma-rays and thermal neutrons for medical and non-destructive testing applications. These compounds are generally characterized by their large energy band-gap. Their high potential as window materials in the ultraviolet (UV) and vacuum ultraviolet (VUV) wavelength region was also identified based on their short absorption edges [12, 13]. CsBaF₃ is an important member of this ternary family of materials because it could be used as a material for lasers when doped with transition metals. It is well known that the materials with band gaps larger than 3.1 eV work well in the ultraviolet (UV) region of the spectrum [14–18]. Since CsBaF₃ is like the other fluoroperovskites and has a wide and direct band gap larger than 7.0 eV, then it can be effectively used in UV based optoelectronic devices. However, there are few studies about this compound and its characteristics have not been investigated in detail up to now [19].

The aim of this work is to investigate the structural, elastic, electronic, optical and thermal properties of fluoro-perovskite CsBaF₃ by the density functional

*corresponding author; e-mail: murtaza@icp.edu.pk

theory using the full potential linearized augmented plane wave (FP-LAPW) method, in order to provide reference data for the experimentalists and to complete existing theoretical and experimental works on this compound.

The rest of the paper has been divided in three parts. In Sect. 2, we briefly describe the computational techniques used in this study. In Sect. 3, we give and discuss our results. Finally, conclusions are given in Sect. 4.

2. Calculation method

The ternary compound CsBaF₃ crystallizes in the cubic perovskite-type structure with space group $Pm\bar{3}m$ (# 221) and its unit cell contains one molecule. The Cs, Ba and F atoms are positioned at: 1a (0,0,0), 1b (1/2,1/2,1/2) and 3c (0,1/2,1/2) sites of the Wyckoff coordinates, respectively.

In this paper, our calculations were carried out using FP-LAPW method [20, 21] implemented in Wien2K computer code [22]. The exchange-correlation potential is treated with the local density approximation (LDA) [23] and the generalized gradient approximation (GGA) [24] to calculate the total energy, while for the electronic and optical properties the recent modified Becke–Johnson potential (TB-mBJ) [25] was also applied. In this method, the space is divided into non-overlapping muffin-tin (MT) spheres separated by an interstitial region. The region of non-overlapping atomic spheres (centered at the atomic sites) is treated as a linear combination of radial functions times spherical harmonics, while in the interstitial region a plane wave expansion is used. For this, a satisfactory degree of convergence was achieved by considering a number of FP-LAPW basis functions up to $R_{\text{MT}}K_{\text{max}}$ equal to 8 (where R_{MT} is the minimum radius of the muffin-tin spheres and K_{max} gives the magnitude of the largest \mathbf{k} -vector in the plane wave expansion). The muffin-tin sphere radii R_{MT} are taken to be 2.5, 2.0, and 1.8 atomic units (a.u.) for Cs, Ba, and F, respectively. The spherical harmonics inside the muffin-tin spheres are expanded up to $l_{\text{max}} = 10$, while the Fourier expanded charge density was truncated at $G_{\text{max}} = 12$ (a.u.)⁻¹. The \mathbf{k} integration over the full Brillouin zone is performed with $8 \times 8 \times 8$ k -points mesh. The self-consistent calculations are considered to be converged when the total energy is stable within 0.1 mRy.

The optical properties can be described the dielectric function $\varepsilon(\omega)$, which is expressed as [26, 27]:

$$\varepsilon(\omega) = \varepsilon_1(\omega) + i\varepsilon_2(\omega). \quad (1)$$

The imaginary part of the dielectric function $\varepsilon_2(\omega)$ was calculated from the electronic band structure of a solid [28]:

$$\varepsilon_2(\omega) = \left(\frac{\hbar^2 e^2}{\pi m^2 \omega^2} \right) \sum_{c,v} \int d^3k \langle c_k | P^\alpha | v_k \rangle \times \langle v_k | P^\beta | c_k \rangle \delta(\varepsilon_{ck} - \varepsilon_{vk} - \omega), \quad (2)$$

where P is the momentum matrix element between states of bands α and β with crystal momentum k . c_k and v_k are the crystal wave functions corresponding to the conduction and the valence bands with crystal wave vector k .

The real part $\varepsilon_1(\omega)$ of the dielectric function can be extracted from the imaginary part using the Kramers–Kronig relation

$$\varepsilon_1(\omega) = 1 + \frac{2}{\pi} \text{P} \int_0^\infty \frac{\omega' \varepsilon_2(\omega')}{\omega'^2 - \omega^2} d\omega'. \quad (3)$$

P is the principle value of the integral. The refractive index $n(\omega)$, the extinction coefficient $k(\omega)$, the absorption coefficient $I(\omega)$ and the reflectivity $R(\omega)$ in the crystal are given by [28]:

$$n(\omega) = \left[\frac{\varepsilon_1(\omega)}{2} + \frac{\sqrt{\varepsilon_1^2(\omega) + \varepsilon_2^2(\omega)}}{2} \right]^{1/2}, \quad (4)$$

$$k(\omega) = \left[-\frac{\varepsilon_1(\omega)}{2} + \frac{\sqrt{\varepsilon_1^2(\omega) + \varepsilon_2^2(\omega)}}{2} \right]^{1/2}, \quad (5)$$

$$I(\omega) = \sqrt{2}\omega \left[\sqrt{\varepsilon_1^2(\omega) + \varepsilon_2^2(\omega)} - \varepsilon_1(\omega) \right]^{1/2}, \quad (6)$$

$$R(\omega) = \frac{n + ik - 1}{n + ik + 1}. \quad (7)$$

The study of thermal effects was done within the quasi-harmonic Debye model implemented in the Gibbs program [29]. For solids described by an energy–volume (E – V) relationship in the static approximations, the Gibbs program allows us to evaluate the Debye temperature to obtain the Gibbs free energy $G(V; P, T)$ and to minimize G for deriving the thermal equation of state (EOS) $V(P, T)$. Other macroscopic properties related to the pressure P and temperature T can be obtained by using some standard thermodynamic relations. Further details of this procedure can be found elsewhere [29–32].

3. Results and discussion

3.1. Structural and elastic properties

Our aim in this subsection is to calculate the total energy as a function of unit-cell volume around the equilibrium cell volume V_0 . The calculated total energies versus volume as shown in Fig. 1 are fitted with the Murnaghan equation of state (EOS) [33] to obtain an analytical interpolation of our computed points from which we determine the ground state properties such as the equilibrium lattice constant a_0 , the bulk modulus B and its pressure derivative B' . Table I gives the computed LDA and GGA equilibrium lattice constant a_0 , bulk modulus B and its pressure derivative B' together with other theoretical values. The calculated lattice constant (bulk modulus) is larger (smaller) than those reported in Ref. [19]. Due to the absence of the experimental results concerning the lattice constant and bulk modulus for the herein studied perovskite, we should support our calculated results on the basis of the known lattice constant and bulk moduli of CsSrF₃ and CsCaF₃. As Cs and F atoms are the same in the three compounds, the lattice constant should be increased with increase of the atomic size of the A element in CsAF₃ (A = Sr, Ca and Ba)

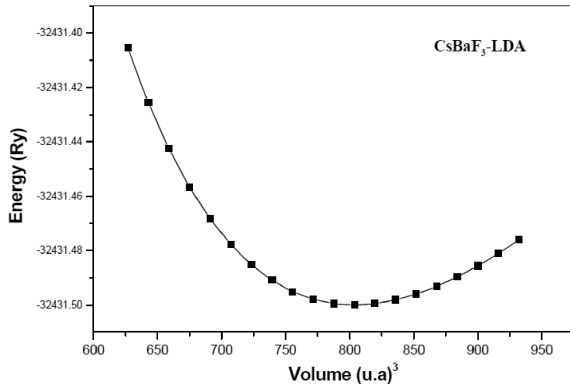


Fig. 1. Variation of total energy versus unit cell volume for CsBaF₃ using LDA approximation.

compounds; $a(\text{CsBaF}_3) > a(\text{CsSrF}_3) > a(\text{CsCaF}_3)$. Following the well-known relationship between B and the lattice constants: $B \propto V_0^{-1}$, where V_0 is the unit cell volume, the bulk modulus values of these compounds should vary in the inverse sequence to lattice constants, i.e. $b(\text{CsCaF}_3) > b(\text{CsSrF}_3) > b(\text{CsBaF}_3)$. The values of lattice constants are 4.40 Å [34], 4.41 Å [35] and 4.52 Å [36] for CsCaF₃ and 4.65 Å [34] and 4.75 Å [37, 38] for CsSrF₃. The bulk modulus values are 67.0 GPa [34] and 65.16 GPa [35] for CsCaF₃ and 53.10 GPa [35] for CsSrF₃. Our calculated lattice constant and bulk modulus of CsBaF₃ follow the above sequences, confirming that our results are more realistic than those quoted in Ref. [19].

TABLE I

Calculated lattice constant (a_0), unit-cell equilibrium volume (V_0), bulk modulus (B) and its pressure derivative B' for CsBaF₃ compound. Results are compared with previous theoretical works.

Properties	Present work		Other theoretical works
	GGA	LDA	
a_0 [Å]	4.97	4.92	4.28 ^a
V_0 [Å ³]	122.76	119.10	-
B [GPa]	42.93	44.55	16.012 ^a
B'	4.09	4.42	-

^aRef. [19]

The elastic constants determine the response of the crystal to the external forces and play an important role for describing the mechanical properties of materials. The values of these constants provide valuable information on the stability and stiffness of materials. For this purpose, the elastic constants of the material of interest has been calculated at zero pressure by computing the components of the stress tensor for small strains, using the derivative of the energy as a function of lattice strain [39] with preserved volume. There are 21 independent elastic constants $C_{i,j}$, but the symmetry of the cubic crystal lattice reduces this number to only three independent elastic constants C_{11} , C_{12} , and C_{44} .

In Table II we summarize the calculated elastic constants and the bulk modulus calculated from the

theoretical elastic constants. From Table II one can remark that the computed LDA elastic constants are higher than those of GGA. This is due to the fact that the LDA bulk modulus value is larger than that of GGA. The requirement of mechanical stability in a cubic crystal leads to the following restrictions on the elastic constants, $C_{11} - C_{12} > 0$, $C_{11} > 0$, $C_{44} > 0$, $C_{11} + 2C_{12} > 0$ [40]. Our calculated C_{ij} values obey these stability conditions, indicating that this compound is elastically stable.

TABLE II

Calculated elastic constants (in GPa), anisotropy factor A , shear modulus G (in GPa), Young's modulus E (in GPa) and the Poisson ratio ν of CsBaF₃.

	C_{11}	C_{12}	C_{44}	A	G	E	ν	B/G
LDA	104.29	15.56	42.51	0.964	43.24	98.32	0.136	1.044
GGA	98.99	15.13	40.73	0.975	41.205	93.73	0.1374	1.045

The elastic anisotropy of crystals has an important implication in engineering science since it is highly correlated with the possibility to induce microcracks in the materials. To quantify the elastic anisotropy of these compounds, we have computed the anisotropy factor $A = 2C_{44}/(C_{11} - C_{12})$ from the present values of the elastic constants. For a completely isotropic material, A is equal to 1, while any value smaller or larger than 1 indicates anisotropy. The magnitude of the deviation from 1 is a measure of the degree of elastic anisotropy possessed by the crystal. The calculated values of the anisotropic factor A are found to be equal to 0.964 with LDA and 0.975 with GGA, meaning that this compound is not characterized by a profound anisotropy.

The elastic constants C_{11} , C_{12} and C_{44} are estimated from first-principles calculations for CsBaF₃ single crystal. However, the prepared material is in general polycrystalline, and therefore it is important to evaluate the corresponding moduli for the polycrystalline species. Using the Voigt–Reuss–Hill approximations, some polycrystalline elastic moduli, namely, the shear modulus G , the Young modulus E and the Poisson ratio ν , have been calculated from the single-crystal elastic constants C_{ij} by the following equations [41–43]:

$$E = \frac{9BG}{3B + G}, \quad (8)$$

$$\nu = \frac{3B - 2G}{2(3B + G)}, \quad (9)$$

$$G_V = \frac{1}{5}(C_{11} - C_{12} + 3C_{44}), \quad (10)$$

$$G_R = \frac{5C_{44}(C_{11} - C_{12})}{4C_{44} + 3(C_{11} - C_{12})}. \quad (11)$$

The calculated values of the mentioned elastic moduli for polycrystalline CsBaF₃ aggregate are given also in Table II. After acquiring the necessary data on the elastic constant, we now try to discuss on the ductility and brittleness of these compounds. There are many factors which allow us to know the ductile/brittle nature

of the given material: Cauchy's pressure ($C_{12} - C_{44}$), Pugh's index of ductility (B/G) and Poisson's ratio (ν). Cauchy's pressure, defined as the difference between the two particular elastic constants $C_{12} - C_{44}$ is considered to serve as an indication of ductility: if the pressure is positive (negative), the material is expected to be ductile (brittle) [44]. Here the value of Cauchy's pressure is found to be equal to -26.9 with LDA and -25.6 with GGA, which clearly highlights the brittle nature of this compound. Another index of ductility is the B/G ratio. According to Pugh's [45] and Frantsevich et al.'s [46] ratios, the high (low) B/G ratio is associated with the ductile (brittle) nature of the materials. The critical number which separates the ductile and brittle was found to be 1.75 (Pugh) and 2.67 (Frantsevich et al.). As mentioned in Table II, this ratio is around 1.04 with both approximations, which also classified this compound as a brittle material. We may also refer to Frantsevich et al. [46] who distinguish the ductility and brittleness of materials in terms of Poisson's ratio (ν). According to Frantsevich rule, the critical value of material is 0.26. For brittle materials, Poisson's ratio is less than 0.26, otherwise the material behaves in a ductile manner, as recently demonstrated in a study of brittle versus ductile transition in some perovskite compounds from first-principles calculations [47, 48]. Here the calculated Poisson value is smaller than 0.26, meaning that this compound is brittle in nature. The more deleterious consequence of brittleness is the sensitivity for thermal shocks, as the material cannot efficiently dissipate thermal stresses via plastic deformations. Thus, a brittle solid can only be subjected to limited thermal shocks before its strength drops dramatically. So we can conclude that the herein studied material is less sensitive to thermal shocks.

3.2. Electronic properties

In this section we turn our attention to study the electronic properties of CsBaF_3 via calculating the energy band structure, the density of states and the charge distribution. It is well known that the LDA and GGA calculations underestimate the fundamental gap of semiconductors and insulators [49–51]. This is mainly due to the fact that they have simple forms that are not sufficiently flexible for accurately reproduce both exchange-correlation energy and its charge derivative. To overcome the underestimation of the band gaps we have applied the modified Becke–Johnson potential (mBJ) which has been applied with successful results in some recent papers [52–54].

The calculated energy band structure for the equilibrium geometry of CsBaF_3 along the higher symmetry directions in the Brillouin zone is shown in Fig. 2. The zero energy is chosen to coincide with the top of the valence band. The results indicated that the energy dispersion of the valence band is very small along a and b axes. On the contrary, large dispersion can be seen along the c -axis. The calculated electronic band structure reveals that CsBaF_3 is an insulator similar to other

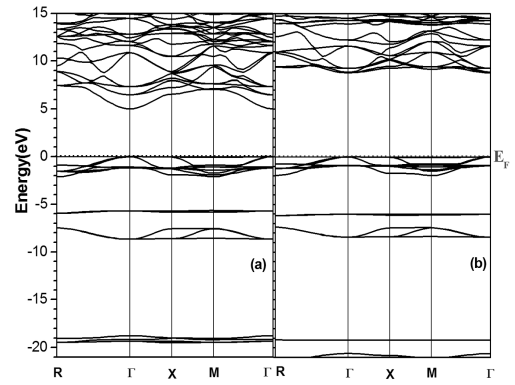


Fig. 2. The calculated band structure in high symmetry directions of CsBaF_3 using (LDA) (a) and (mBJ) (b).

fluoroperovskites [48, 55–58]. The nine valence bands between -2.0 eV and the Fermi level (zero) are mainly due to p orbital of fluorine atoms. The upper valence band situated between -2.0 eV and Fermi level is constituted by nine bands. These nine valence bands are split into threefold degenerate levels at the Γ point (Γ_{15} , Γ_{25} , and Γ_{15}) separated by energies of 1.106 eV ($\Gamma_{15} - \Gamma_{25}$) and 0.086 eV ($\Gamma_{25} - \Gamma_{15}$). The split of these levels is produced by the crystalline field and the electrostatic interactions between F $2p$ orbitals. CsBaF_3 has the conduction band minimum (CBM) and the valence band maximum (VBM) at the Γ point, resulting in a direct band gap ($\Gamma - \Gamma$). The calculated values of the band gaps are found to be equal to 4.94 eV. The calculated values of the main direct and indirect band gaps at zero pressure are given in Table III.

TABLE III

Calculated energy gaps at high symmetry points for CsBaF_3 compound (energies are in eV).

	$R-R$	$\Gamma-\Gamma$	$X-X$	$M-M$	$R-\Gamma$
LDA	8.35	5.02	6.60	7.09	5.91
GGA	8.14	4.95	6.53	6.99	5.72
mBJ	10.13	8.78	9.31	9.23	9.41

To obtain a deeper insight into the electronic structure, we have displayed in Fig. 3 the total and the partial atomic density of states (TDOS and PDOS) for CsBaF_3 . Starting from the lower energy side, the deep electronic localized structure centered at around -22 eV, below the Fermi level is due to near equal contributions of F s and Ba s states. The structure situated at around -8 eV consists of Ba p states. The structure situated at around -6 eV arises mainly from Cs p states. The upper valence band situated between -2 and 0 eV is essentially formed by F p states with a small contribution of Ba d and p states. The bottom of the conduction bands are essentially dominated by Cs d states hybridized with Ba d states with a small contribution of F p states.

In order to further explore the bonding nature in the cubic CsBaF_3 , the charge distribution in this compound

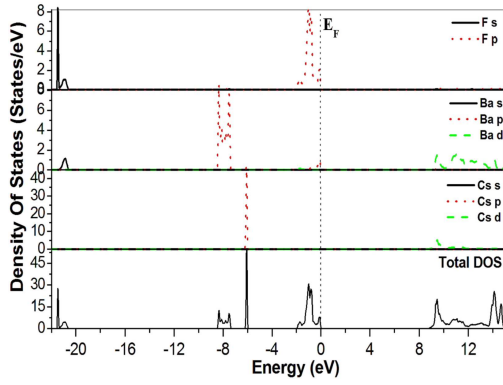


Fig. 3. The calculated total and partial densities of states (DOS) of CsBaF₃ using the mBJ approximation.

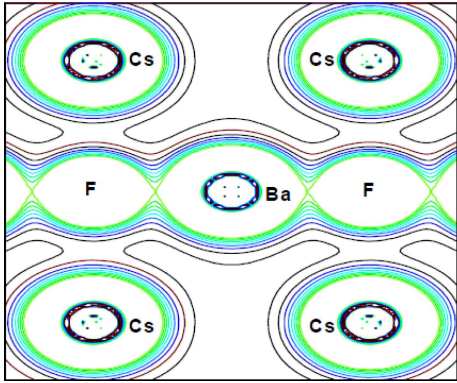


Fig. 4. The calculated charge density along the [1 1 0] direction of CsBaF₃ at the predicted equilibrium lattice constant.

is examined. The contour map of the charge density in (110) plane, containing caesium (Cs), barium (Ba) and fluoride (F) atoms, is shown in Fig. 4. From this figure one can see that the highest charge density resides in the immediate vicinity of the nuclei. The near spherical charge distribution around the Cs indicates that the bonding between Cs and F is predominantly ionic. This figure reveals a sharing of charge between Ba and F due to the Ba *d* and F *p* hybridization; thus, there is a mixture of covalent-ionic bonding between Ba and F.

3.3. Optical properties

All the optical properties are calculated at the theoretical equilibrium lattice constant for the energy up to 35 eV. Figure 5 shows the calculated real part (the dispersive part) of the dielectric function $\varepsilon_1(\omega)$. The main peak is about at 15.30 eV for CsBaF₃. The curve shows decreases followed by increases and then decreases to reach $\varepsilon_1(\omega)$ negative value; followed by a slow increase toward zero at high energy. The calculated static dielectric constant $\varepsilon_1(0)$ is about 2.01. We note that the zero's value of $\varepsilon_1(\omega)$ ($\varepsilon_1 = 0$), which reflects the absence of the dispersion coincides perfectly with the maximum of the absorption coefficient $I(\omega)$ (Fig. 6), which is situated at 15.66 eV.

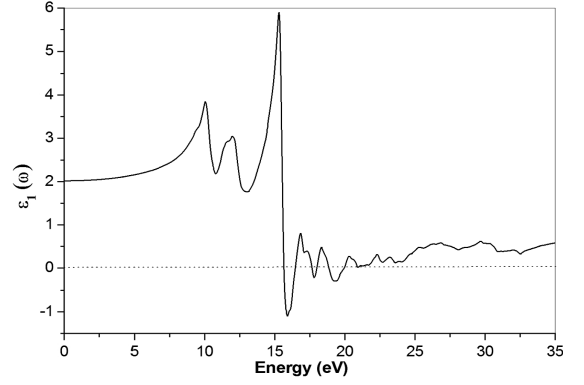


Fig. 5. The calculated real part of the dielectric function $\varepsilon_1(\omega)$ of CsBaF₃.

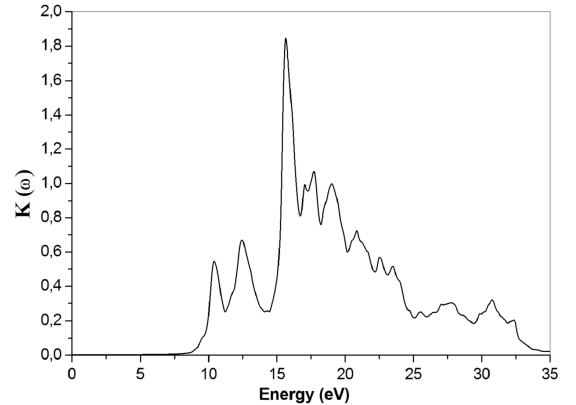


Fig. 6. The calculated extinction coefficient $k(\omega)$ of CsBaF₃.

The imaginary part of the dielectric function $\varepsilon_2(\omega)$ is calculated from the momentum matrix elements between the occupied and unoccupied wave functions within the selection rules. Figure 7 displays the calculated imaginary part of the dielectric function for CsBaF₃ for a radiation up to 35 eV. Our analysis of $\varepsilon_2(\omega)$ spectrum shows that the first critical points (threshold energy) of the dielectric function occur at about 8.77 eV. This point is the direct optical transitions between the highest valence band and the lowest conduction band at the Γ -point. This is known as the fundamental absorption edge. Beyond this point, the curve increases rapidly due to the abrupt increase in the number of points contributing toward $\varepsilon_2(\omega)$. The main peak in the spectrum is situated at 10.32 eV for CsBaF₃. This peak is dominated by the direct optical transitions from F 2*p* band just below the Fermi energy to Ba 5*d* state of conduction band. All structures in the optical response are in agreement with the band structure. The optical band gap obtained from the imaginary part of the dielectric function is 8.77 eV which is closer to that obtained from the electronic band structure (8.78 eV). Hence, the direct wide band gap nature makes the compound suitable for the high frequency UV devices applications.

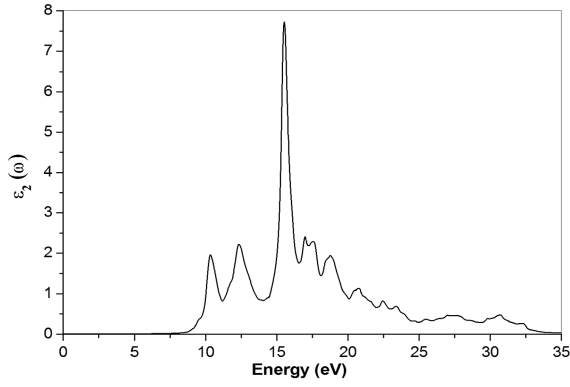


Fig. 7. The calculated imaginary part of the dielectric function $\varepsilon_2(\omega)$ of CsBaF₃.

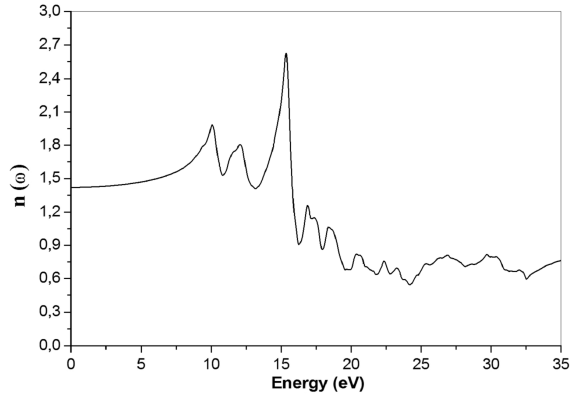


Fig. 8. The calculated refractive index $n(\omega)$ of CsBaF₃.

The knowledge of $\varepsilon_1(\omega)$ and $\varepsilon_2(\omega)$ allows the calculation of refractive index $n(\omega)$, extinction coefficient $k(\omega)$, absorption coefficient $I(\omega)$ and reflectivity $R(\omega)$. The calculated refractive index $n(\omega)$ and the extinction coefficient $k(\omega)$ are shown in Figs. 8 and 6, respectively. The refractive index spectrum indicates that the static refractive index $n(0)$ has a value of 1.42. All peaks of the refractive index and extinction coefficient coincide with a slight shift.

The absorption coefficient $I(\omega)$ is investigated in Fig. 9. High absorption peaks at high energies are noticeable. The maximum absorption coefficient is found around 15.66 eV. This material possesses considerable absorption.

Figure 10 shows the calculated reflectivity $R(\omega)$. From this curve, the reflectivity indicates a maximum peak at around 15.71 eV. The zero frequency limit of reflectivity for CsBaF₃ is found to be 0.03. There are high reflection peaks at energies 15.71 eV, 17.81 eV and 19.47 eV corresponding to the negative values of $\varepsilon_1(\omega)$. In the energy range up to the band gap the reflectivity is very small, and therefore the material is transparent for the incident photons; hence, the materials also show the transparency for this energy range which suggests this compound as promising candidate for making lenses.

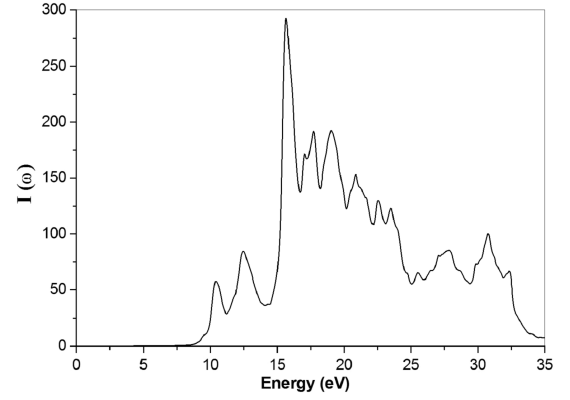


Fig. 9. The calculated absorption coefficient $I(\omega)$ of CsBaF₃.

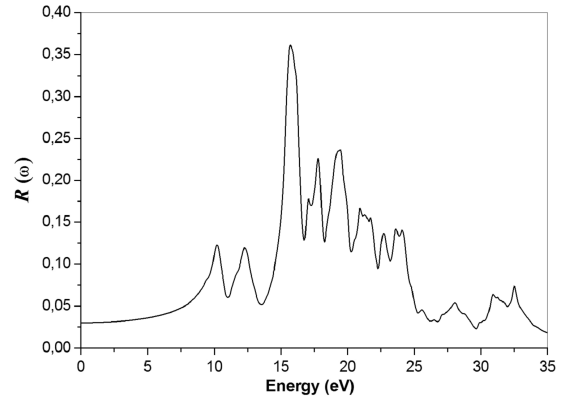


Fig. 10. The calculated reflectivity $R(\omega)$ of CsBaF₃.

3.4. Thermodynamic properties

To investigate the thermal properties of CsBaF₃ compound under high temperature and high pressure, we have applied the quasi-harmonic Debye approximation. As a first step, a set of total energy calculation versus unit cell volume $E-V$, in the static approximation, was carried out and fitted with the numerical EOS in order to determine its structural parameters at zero temperature and pressure, and then derive the macroscopic properties as function of pressure and temperature from standard thermodynamic relations. The thermal properties are determined in the temperature range from 0 to 1000 K where the quasi-harmonic model remains fully valid. The pressure effect is studied in the 0–40 GPa range. Figure 11a and b displays the variation of the unit cell volume V and the bulk modulus as a function of temperature at different pressures for CsBaF₃. One can remark that at a given pressure both volume and bulk modulus are nearly constant from 0 to 100 K. Above this temperature ($T > 100$ K), the unit cell volume V increases and the bulk modulus decreases with increasing temperature. On the other side as the pressure P increases the unit cell volume V decrease and the bulk modulus increases at a given temperature. These results are due to the fact that the effect of increasing pressure of the material is the same as the decreasing temperature of the material.

The compressibility increases with increasing temperature at a given pressure and decreases with pressure at a given temperature. The calculated equilibrium unit cell volume V and bulk modulus at zero pressure and room temperature are 122.28 \AA^3 and 39.85 GPa , respectively.

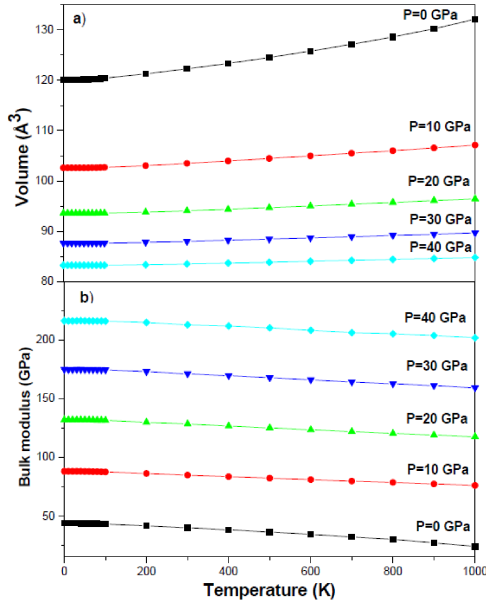


Fig. 11. The variation of the unit cell volume (a) and bulk modulus (b) as a function of temperature at different pressures for CsBaF_3 .

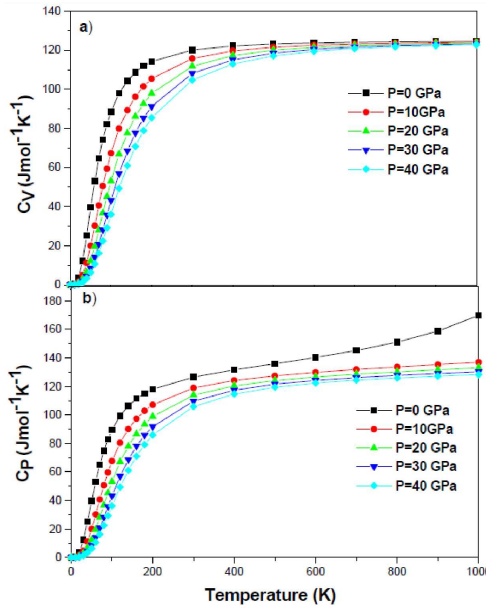


Fig. 12. The variation of the heat capacities C_V (a) and (b) as a function of temperature at different pressures for CsBaF_3 .

The knowledge of the heat capacity of a substance provides essential insight into its vibrational properties and is also mandatory for many applications, so the variation of the heat capacity at constant volume C_V versus

temperature at 0, 10, 20, 30 and 40 GPa pressures for CsBaF_3 is shown in Fig. 12a. It is worth mentioning from this figure that C_V curve shows a sharp increase up to 300 K, and then increase slowly in the high temperature. At high temperature C_V is close to a constant value $123.75 \text{ J mol}^{-1} \text{ K}^{-1}$, which is the so-called Dulong–Petit limit [59], which is common to all solids at high temperature. In view in Fig. 12a, it is clear that when ($T < 500 \text{ K}$), the heat capacity C_V depends on both temperature and pressure (C_V is proportional to T^3 [60]). The variation of the heat capacity exhibits a similar feature in wide temperature and pressure. Figure 12b displays the heat capacity C_p as a function of temperature for various pressures. It is shown that when ($T < 400 \text{ K}$), the variation features of C_p values are similar to that of C_V . Furthermore, C_V and C_p are depending on both temperature and pressure and increase exponentially. However in the high-temperature range ($T > 400 \text{ K}$) the change of C_p is different than that of C_V . C_p values decrease with increasing pressure and do not converge to a constant value. The heat capacity C_p increases rapidly at high temperature. At room temperature and zero pressure the C_p value is found to be equal to $126.56 \text{ J mol}^{-1} \text{ K}^{-1}$.

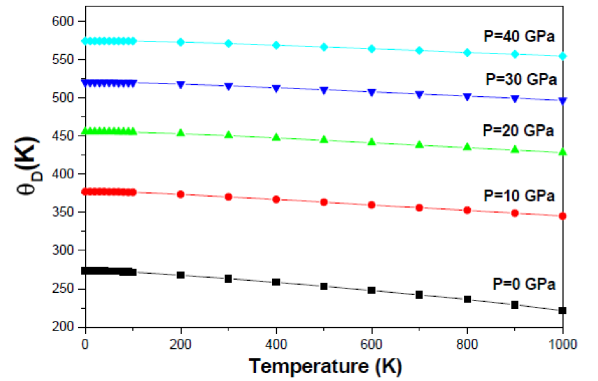


Fig. 13. The variation of the Debye temperature as a function of temperature at different pressures for CsBaF_3 .

The Debye temperature θ_D is an important parameter, characteristic for the thermal properties of solids. It is the temperature above which the crystal behaves classically, because the thermal vibrations become more important than the quantum effects. Figure 13 shows the evolution of the Debye temperature θ_D with temperature at several fixed pressures. It can be seen that θ_D is nearly constant from 0 to 200 K and decreases linearly with increasing temperature. For a fixed temperature, the Debye temperature increases with the enhancement of pressure. Our calculated θ_D at zero pressure and ambient temperature is found to be equal to 263.27 K . This might be an indication that the quasi-harmonic Debye model is a very reasonable alternative to account for the thermal effects with no expensive task in terms of computational time.

4. Conclusions

In this work, we have performed *ab initio* calculations on the structural, elastic, electronic, optical and thermodynamic properties for the cubic CsBaF₃ using the FP-LAPW method with LDA, GGA and the modified Becke–Johnson potential. The most relevant results are summarized as follows:

- The calculated ground-state properties such as lattice constant and bulk modulus agree well with other theoretical works.
- We have predicted some elastic properties such as elastic constants, anisotropy factor, shear modulus, Young's modulus and Poisson's ratio. The B/G ratio indicates that CsBaF₃ is brittle in nature.
- On the basis of the direct wide band gap and the spectra of imaginary part of the dielectric function it can be concluded that this material will be useful for optoelectronic applications in the UV region.
- Through the quasi-harmonic Debye model, the dependences of the volume, bulk modulus, heat capacities and Debye temperature on temperature and pressure have been obtained successfully.

Acknowledgments

R. Khenata and S. Bin-Omran acknowledge the financial support by the Deanship of Scientific Research at King Saud University for funding the work through the research group project No. RPG-VPP-088. For author H. Khachai this work has been supported by the Algerian national research projects PNR (No. 8/U310/4153).

References

- [1] W.S. Kim, E.O. Chi, J.C. Kim, H.S. Choi, N.H. Hur, *Solid State Commun.* **119**, 507 (2001).
- [2] E.O. Chi, W.S. Kim, N.H. Hur, *Solid State Commun.* **120**, 307 (2001).
- [3] T.M. Bloomstein, V. Liberman, M. Rotschild, D.E. Hardy, R.B. Goodman, *Proc. SPIE* **3676**, 342 (1999).
- [4] H. Manaa, Y. Guyot, R. Moncorge, *Phys. Rev. B* **48**, 3633 (1993).
- [5] J.M. Garcia-Lastra, J.Y. Buzaré, M.T. Barriuso, J.A. Aramburu, M. Moreno, *Phys. Rev. B* **75**, 155101 (2007).
- [6] M.C.M. de Lucas, F. Rodriguez, M. Moreno, *J. Phys. Condens. Matter* **7**, 7535 (1995).
- [7] C.N. Avram, M.G. Brik, I. Tanaka, N.M. Avram, *Physica B* **355**, 164 (2005).
- [8] F. Lahoz, B. Villacampa, R. Alcalá, *J. Phys. Chem. Solids* **58**, 881 (1997).
- [9] P. Berastegui, S. Hull, S.-G. Eriksson, *J. Phys. Condens. Matter* **13**, 5077 (2001).
- [10] J. Julliard, J. Nouet, *Rev. Phys. Appl.* **10**, 325 (1975).
- [11] R.R. Daniels, G. Margaritondo, R.A. Heaton, C.C. Lin, *Phys. Rev. B* **27**, 3878 (1983).
- [12] K. Shimamura, T. Fujita, H. Sato, A. Bensalah, N. Sarukura, T. Fukuda, *Jpn. J. Appl. Phys.* **39**, 6807 (2000).
- [13] A. Bensalah, K. Shimamura, K. Nakano, T. Fujita, T. Fukuda, *J. Cryst. Growth* **231**, 143 (2001).
- [14] M. Maqbool, I. Ahmad, H.H. Richardson, M.E. Kordesch, *Appl. Phys. Lett.* **91**, 193511 (2007).
- [15] G. Murtaza, I. Ahmad, *J. Appl. Phys.* **111**, 123116 (2012).
- [16] M. Maqbool, M.E. Kordesch, A. Kayani, *J. Opt. Soc. Am. B* **26**, 998 (2009).
- [17] G. Murtaza, Iftikhar Ahmad, B. Amin, A. Afaq, M. Maqbool, J. Maqssod, I. Khan, M. Zahid, *Opt. Mater.* **33**, 553 (2011).
- [18] B. Amin, I. Ahmad, M. Maqbool, *J. Lightwave Technol.* **28**, 223 (2010).
- [19] azufre.quimica.uniovi.es/acc/seminario.pdf.
- [20] G.K.H. Madsen, P. Blaha, K. Schwarz, E. Sjöstedt, L. Nordström, *Phys. Rev. B* **64**, 195134 (2001).
- [21] K. Schwarz, P. Blaha, G.K.H. Madsen, *Comput. Phys. Commun.* **147**, 71 (2002).
- [22] P. Blaha, K. Schwarz, G.K.H. Madsen, D. Kvasnicka, J. Luitz, *Wien2k, An Agmented Plane Wave Plus Local Orbitals Program for Calculating Crystal Properties*, Vienna University of Technology, Austria 2001.
- [23] J.P. Perdew, Y. Wang, *Phys. Rev. B* **45**, 13244 (1992).
- [24] J.P. Perdew, K. Burke, M. Ernzerhof, *Phys. Rev. Lett.* **77**, 3865 (1996).
- [25] F. Tran, P. Blaha, *Phys. Rev. Lett.* **102**, 226401 (2009).
- [26] J.S. Tell, *Phys. Rev.* **104**, 1760 (1956).
- [27] C. Ambrosch-Draxl, J.O. Sofo, *Comput. Phys. Commun.* **175**, 1 (2006).
- [28] M. Dressel, G. Gruner, *Electrodynamics of Solids: Optical Properties of Electrons in Matter*, Cambridge University Press, UK 2002.
- [29] M.A. Blanco, E. Francisco, V. Luana, *Comput. Phys. Commun.* **158**, 57 (2004).
- [30] M.A. Blanco, A.M. Pendás, E. Francisco, J.M. Recio, R. Franco, *J. Mol. Struct. Theochem.* **368**, 245 (1996).
- [31] M. Florez, J.M. Recio, E. Francisco, M.A. Blanco, A.M. Pendás, *Phys. Rev. B* **66**, 144112 (2002).
- [32] E. Francisco, M.A. Blanco, G. Sunjurjo, *Phys. Rev. B* **63**, 049107 (2001).
- [33] F.D. Murnaghan, *Proc. Natl. Acad. Sci. USA* **30**, 244 (1944).
- [34] A. Meziani, H. Belkhir, *Computat. Mater. Sci.* **61**, 67 (2012).
- [35] B. Ghebouli, M.A. Ghebouli, A. Bouhemadou, M. Fatmi, R. Khenata, D. Rached, T. Ouahrani, S. Bin-Omran, *Solid State Sci.* **14**, 903 (2012).
- [36] C. Ridou, M. Rousseau, J. Bouillot, C. Vettier, *J. Phys. E* **55**, 291 (1984).

- [37] R.L. Moreira, A. Dias, *J. Phys. Chem. Solids* **68**, 1617 (2007).
- [38] Hayatullah, S. Naeem, G. Murtaza, R. Khenata, M.N. Khalid, *Physica B* **414**, 91 (2013).
- [39] M.J. Mehl, *Phys. Rev. B* **47**, 2493 (1993).
- [40] J. Wang, S. Yip, S. R. Phillpot, and Dieter Wolf *Phys. Rev. Lett.* **71**, 4182 (1993).
- [41] R. Hill, *Proc. Phys. Soc. Lond. A* **65**, 349 (1952).
- [42] W. Voigt, *Handbook of Crystal Physics*, Teubner, Leipzig 1928.
- [43] A. Russ, A. Angew, *Mater. Phys.* **9**, 49 (1929).
- [44] D.G. Pettifor, *Mater. Sci. Technol.* **8**, 345 (1992).
- [45] S.F. Pugh, *Philos. Mag.* **45**, 823 (1954).
- [46] I.N. Frantsevich, F.F. Voronov, S.A. Bokuta, in: *Elastic Constants and Elastic Moduli of Metals and Insulators Handbook*, Ed. I.N. Frantsevich, Naukova Dumka, Kiev 1983, p. 60.
- [47] G. Vaitheeswaran, V. Kanchana, A. Svane, A. Delin, *J. Phys. Condens. Matter* **19**, 326214 (2007).
- [48] G. Vaitheeswaran, V. Kanchana, R.S. Kumar, A.L. Cornelius, M.F. Nicol, A. Svane, A. Delin, B. Johansson, *Phys. Rev. B* **76**, 014107 (2007).
- [49] P. Dufek, P. Blaha, K. Schwarz, *Phys. Rev. B* **50**, 7279 (1994).
- [50] Z. Charifi, H. Baaziz, F. El Haj Hassan, N. Bouarissa, *J. Phys. Condens. Matter.* **17**, 4083 (2005).
- [51] F. El Haj Hassan, H. Akbarzadeh, S.J. Hashemifar, A. Mokhtari, *J. Phys. Chem. Solids* **65**, 1871 (2004).
- [52] A.H. Reshak, S. Auluck, M. Piasecki, G.L. Myronchuk, O. Parasyuk, I.V. Kityk, H. Kamarudin, *Spectrochim. Acta A* **93**, 274 (2012).
- [53] A. Manzar, G. Murtaza, R. Khenata, S. Muhammad, Hayatullah, *Chin. Phys. Lett.* **30**, 047401 (2013).
- [54] A.H. Reshak, H. Kamarudin, S. Auluck, *J. Phys. Chem. B* **116**, 4677 (2012).
- [55] T. Nishimatsu, N. Terakubo, H. Mizuseki, Y. Kawazoe, D.A. Pawlak, K. Shimamuri, T. Fukuda, *Jpn. J. Appl. Phys.* **41**, 365 (2002).
- [56] G. Vaitheeswaran, V. Kanchana, R.S. Kumar, A.L. Cornelius, M.F. Nicol, A. Svane, N.E. Christensen, O. Eriksson, *Phys. Rev. B* **81**, 075105 (2010).
- [57] T. Seddik, R. Khenata, O. Merabiha, A. Bouhemadou, S. Bin-Omran, D. Rached, *Appl. Phys. A* **106**, 645 (2012).
- [58] Hayatullah, G. Murtaza, R. Khenata, S. Naeem, M.N. Khalid, S. Mohammad, *Chin. Phys. Lett.* **30**, 097101 (2013).
- [59] A.T. Petit, P.L. Dulong, *Ann. Chim. Phys.* **10**, 395 (1819).
- [60] P. Debye, *Ann. Phys.* **39**, 789 (1912).